

Extended Gravitational Decoupled Solutions in Self-interacting Brans-Dicke Theory

M. Sharif ^{*} and Amal Majid [†]

Department of Mathematics, University of the Punjab,
Quaid-e-Azam Campus, Lahore-54590, Pakistan.

Abstract

In this paper, we construct anisotropic spherical solutions from known isotropic solutions through extended gravitational decoupling method in the background of self-interacting Brans-Dicke theory. The field equations are decoupled into two sets by applying geometric deformations on radial as well as temporal metric components. The first array corresponds to isotropic fluid while influence of the anisotropic source is confined to the second set. The isotropic sector is determined through metric functions of isotropic solutions (Tolman IV/Krori-Barua) whereas two constraints on the anisotropic source are required to close the second system. The impact of the massive scalar field as well as the decoupling parameter on the physical characteristics of the anisotropic solutions is analyzed graphically. We also check the viability, compactness, surface redshift and stability of the obtained solutions. It is found that the resulting solutions follow accepted physical trend for some values of the decoupling parameter.

Keywords: Brans-Dicke theory; Gravitational decoupling; Self-gravitating systems.

PACS: 04.50.Kd; 04.40.-b; 04.40.Dg

^{*}msharif.math@pu.edu.pk

[†]amalmajid89@gmail.com

1 Introduction

The universe is a well-structured yet incomprehensible system composed of heavenly bodies and other mysterious components. The key to understand the evolution of the vast cosmos lies in the study of the arrangement as well as the physical behavior of celestial objects. In this regard, general relativity (GR) played a remarkable role in providing elementary insights to the mechanism governing the interior of astronomical bodies. The exact solutions of the non-linear field equations describe the intricate nature of relativistic objects. Schwarzschild [1], the pioneer, obtained a solution describing a spherical object with an incompressible perfect fluid in its interior. Many researchers followed suit and constructed more interior solutions. However, the non-linearity of the equations poses a hindrance to extracting physically realistic solutions.

Lemaitre [2] observed that anisotropy occurs in low as well as high-density profiles due to rotational motion, phase transition, or presence of magnetic field, or viscous fluid. Later, in 1972, Ruderman [3] proposed that nuclear interactions within extremely dense systems generate anisotropy. Since observations of astrophysical structures reveal high nuclear density at their cores, therefore, anisotropy is one of the salient features of their intrinsic geometries and evolution. Researchers have considered radial and tangential components of pressure to incorporate anisotropy in the structure of stellar objects. Herrera and Santos [4] investigated possible factors that induce anisotropy in spherical systems in GR. Static solutions describing the anisotropic interior of cosmic objects were derived by Harko and Mak [5] through a particular form of anisotropy factor. Paul and Deb [6] evaluated physically acceptable anisotropic solutions of systems in hydrostatic equilibrium by considering observed masses of compact stars. Murad [7] incorporated the effects of the electromagnetic field to model anisotropic strange stars by considering a specific form of the metric potential.

Over the years, researchers have devised new techniques to obtain viable models of stellar structures. Recently, Ovalle [8] proposed the method of minimal geometric deformation (MGD) to extend a seed source (vacuum or isotropic) to complex fluid distributions. This technique was first implemented in the framework of Randall-Sundrum braneworld to derive consistent spherically symmetric solutions. In this approach, an additional source is incorporated in the seed distribution on the condition that the two sources interact gravitationally only. A geometric deformation in the radial metric

component decouples the system of field equations into two sets with lesser degrees of freedom as compared to the original system. The two systems are solved independently and their respective solutions are combined to obtain a solution of the complete model.

Following the procedure of MGD, Ovalle and Linares [9] computed the braneworld version of Tolman IV and inspected the bulk effects on the compactness of self-gravitating objects. Ovalle et al. [10] employed this technique to incorporate the effects of anisotropy in perfect fluid configuration and generated three anisotropic models from the Tolman IV solution. Gabbanelli et al. [11] discussed the salient features of anisotropic version of the Durgapal-Fuloria solution. Estrada and Tello-Ortiz [12] adopted the MGD approach to construct two physically acceptable anisotropic solutions from Heintzmann solution. Sharif and Sadiq [13] applied this method to Krori-Barua (KB) solution and explored the impact of charge on the extended anisotropic system. Geometric deformations on Tolman VII metric potentials have also been applied to construct a physically viable anisotropic solution [14]. Sharif and Ama-Tul-Mughani [15] decoupled the field equations representing a cloud of strings and obtained corresponding anisotropic extensions.

Although gravitational decoupling via MGD is a highly effective scheme for constructing viable solutions of the field equations. However, deformation in the radial metric component splits the field equations only when the exchange of energy and momentum between the considered sources is restricted. In order to overcome this shortcoming, Casadio et al. [16] modified the MGD technique by introducing deformations in radial as well as temporal metric components. However, this extension is valid only in the absence of matter and does not satisfy the Bianchi identities corresponding to self-gravitating systems filled with fluid. Recently, Ovalle [17] presented the most general way of decoupling a spherical system by geometrically deforming both (temporal/radial) metric functions. The main advantage of extended geometric deformation (EGD) decoupling is that it works for all regions of spacetime without imposing any restriction on the choice of matter distribution. Contreras and Bargeño [18] employed this technique in 2+1-dimensions and extended vacuum BTZ solution to an exterior charged BTZ solution. Sharif and Ama-Tul-Mughani implemented EGD approach to generate anisotropic analogues of Tolman IV [19] and KB [20] solutions. Recently, MGD as well as EGD approaches have been used to obtain anisotropic solutions in modified theories as well [21].

In 1937, Dirac [22] hypothesized that all large numbers obtained by the

combinations of fundamental atomic constants are related to cosmological parameters. Subsequently, the gravitational constant G must be a function of cosmic time. In 1961, Brans and Dicke [23] modified GR by incorporating Dirac observations in a scalar-tensor theory and formulated a spherical vacuum solution. Brans-Dicke (BD) gravity incorporates a massless scalar field $\varphi = \frac{1}{G(t)}$ to discuss the evolution of the cosmos. A tunable parameter (ω_{BD}) couples the scalar field to the matter distribution. As the role of scalar field is enhanced during the inflationary era, the values of the coupling parameter must be small to explain this scenario [24]. On the other hand, the solar system tests are satisfied for $\omega_{BD} > 40,000$ [25]. This issue is resolved by the self-interacting BD (SBD) theory which assigns a mass to the scalar field through a potential function $V(\Psi)$ (where Ψ is a massive scalar field) [26]. In SBD theory, if the mass of the scalar field is greater than $2 \times 10^{-25} GeV$, the solar system observations cannot constrain ω_{BD} and its values greater than $-\frac{3}{2}$ are allowed [27].

Solutions representing different scenarios have been formulated in BD theory. Buchdahl [28] considered spherical as well as axially symmetric spacetimes to show that a static vacuum solution of GR can generate a family of static vacuum solutions in BD theory. Sneddon and McIntosh [29] extended Buchdahl work by applying Geroch method [30] to construct new vacuum solutions. Bruckman and Kazes [31] applied a linear equation of state (EoS) to perfect fluid model and formulated an exact spherical solution with infinite density at the center. Goswami [32] constructed a class of vacuum solutions by converting the BD field equations to Einstein vacuum field equations. This work was extended to evaluate solutions in the presence of electromagnetic field as well as an irrotational barotropic fluid [33]. A Demiański-type metric was obtained via a complex coordinate transformation by Krori and Bhattacharjee [34]. Riazi and Askari [35] approximated spherically symmetric solutions for a static vacuum spacetime and examined the behavior of rotation curves. Recently, isotropic versions of Durgapal-Fuloria and KB solutions were extended to anisotropic domain through MGD approach in the context of SBD theory [36].

The realistic models of relativistic stars have extensively been discussed in scalar-tensor theories. Yazadjiev et al. [37] explored how the structure of slowly rotating neutron stars deviate from the GR model in the presence of a massive scalar field. Ramazanoğlu and Pretorius [38] reviewed the range allowed for mass and scalarization of neutron stars by allotting a mass to the scalar field. Doneva and Yazadjiev [39] investigated the dynamics of rapidly

rotating neutron stars in the presence of a massive scalar field and concluded that deviations from GR can be large due to moment of inertia. Staykov et al. [40] extended this work by considering a self-interacting potential along with a massive scalar field to analyze the behavior of static and slowly rotating neutron stars. Popchev et al. [41] analyzed the effects of a self-interacting massive scalar field on moment of inertia and compactness of slowly rotating neutron stars by employing different EoS.

The focus of this paper is to evaluate viable anisotropic versions of Tolman IV and KB solutions by decoupling the SBD field equations via the EGD approach. The paper is organized as follows. In section 2, we construct the field equations by introducing an anisotropic source in perfect fluid distribution which are then decoupled in section 3. Extended anisotropic solutions are computed through some physical constraints and examined for viability in section 4. In the last section, the main results are summarized.

2 Self-interacting Brans-Dicke Theory

The modified action of SBD theory with an additional source in relativistic units ($8\pi G_0 = 1$) is given by

$$S = \int \sqrt{-g} (\mathcal{R}\Psi - \frac{\omega_{BD}}{\Psi} \nabla^\gamma \nabla_\gamma \Psi - V(\Psi) + L_m + \alpha L_\Theta) d^4x, \quad (1)$$

where \mathcal{R} is the Ricci scalar, L_m and L_Θ represent Lagrangian densities of matter and new source, respectively. Moreover, the additional source ($\Theta_{\gamma\delta}$) is coupled to the matter distribution through a dimensionless parameter α . The new source generally induces anisotropy in an isotropic self-gravitating system by including scalar, vector or tensor fields in the stellar model. The SBD field equations and wave equation, obtained from the above action, are respectively given as

$$G_{\gamma\delta} = T_{\gamma\delta}^{(\text{eff})} + \frac{\alpha}{\Psi} \Theta_{\gamma\delta} = \frac{1}{\Psi} (T_{\gamma\delta}^{(m)} + T_{\gamma\delta}^\Psi + \alpha \Theta_{\gamma\delta}), \quad (2)$$

$$\square \Psi = \frac{\bar{T}}{3 + 2\omega_{BD}} + \frac{1}{3 + 2\omega_{BD}} (\Psi \frac{dV(\Psi)}{d\Psi} - 2V(\Psi)), \quad (3)$$

where \square denotes the d'Alembertian operator. The interior configuration of a compact object filled with perfect fluid is represented by the following

energy-momentum tensor

$$T_{\gamma\delta}^{(m)} = (\rho + p)u_\gamma u_\delta - pg_{\gamma\delta}, \quad (4)$$

where ρ , p and u_γ denote energy density, isotropic pressure and four velocity, respectively. Also, $\bar{T} = \Theta + T^{(m)}$, ($\Theta = g^{\gamma\delta}\Theta_{\gamma\delta}$, $T^{(m)} = g^{\gamma\delta}T_{\gamma\delta}^{(m)}$). The energy-momentum tensor related to the massive scalar field is defined as

$$T_{\gamma\delta}^\Psi = \Psi_{,\gamma;\delta} - g_{\gamma\delta}\square\Psi + \frac{\omega_{BD}}{\Psi}(\Psi_{,\gamma}\Psi_{,\delta} - \frac{g_{\gamma\delta}\Psi_{,\alpha}\Psi^{,\alpha}}{2}) - \frac{V(\Psi)g_{\gamma\delta}}{2}. \quad (5)$$

The internal geometry of a static spherical object is described by the line element

$$ds^2 = e^{v(r)}dt^2 - e^{\chi(r)}dr^2 - r^2(d\theta^2 + \sin^2\theta d\phi^2). \quad (6)$$

The field equations incorporating the anisotropic source are formulated via Eqs.(2)-(6) as

$$\frac{1}{r^2} - e^{-\chi} \left(\frac{1}{r^2} - \frac{\chi'}{r} \right) = \frac{1}{\Psi}(\rho + \alpha\Theta_0^0 + T_0^{0\Psi}), \quad (7)$$

$$-\frac{1}{r^2} + e^{-\chi} \left(\frac{1}{r^2} + \frac{v'}{r} \right) = \frac{1}{\Psi}(p - \alpha\Theta_1^1 - T_1^{1\Psi}), \quad (8)$$

$$\frac{e^{-\chi}}{4} \left(2v'' + v'^2 - \chi'v' + 2\frac{v' - \chi'}{r} \right) = \frac{1}{\Psi}(p - \alpha\Theta_2^2 - T_2^{2\Psi}), \quad (9)$$

where

$$\begin{aligned} T_0^{0\Psi} &= e^{-\chi} \left[\Psi'' + \left(\frac{2}{r} - \frac{\chi'}{2} \right) \Psi' + \frac{\omega_{BD}}{2\Psi} \Psi'^2 - e^\chi \frac{V(\Psi)}{2} \right], \\ T_1^{1\Psi} &= e^{-\chi} \left[\left(\frac{2}{r} + \frac{v'}{2} \right) \Psi' - \frac{\omega_{BD}}{2\Psi} \Psi'^2 - e^\chi \frac{V(\Psi)}{2} \right], \\ T_2^{2\Psi} &= e^{-\chi} \left[\Psi'' + \left(\frac{1}{r} - \frac{\chi'}{2} + \frac{v'}{2} \right) \Psi' + \frac{\omega_{BD}}{2\Psi} \Psi'^2 - e^\chi \frac{V(\Psi)}{2} \right]. \end{aligned}$$

Here prime denotes differentiation with respect to r . The evolution equation (3) for the metric (6) turns out to be

$$\square\Psi = -e^{-\chi} \left[\left(\frac{2}{r} - \frac{\chi'}{2} + \frac{v'}{2} \right) \Psi' + \Psi'' \right]. \quad (10)$$

For $\Theta_1^1 \neq \Theta_2^2$, the anisotropy introduced by the extra source is $\Delta = T_2^{2(\text{eff})} - T_1^{1(\text{eff})}$. This work is carried out by choosing the following potential function

$$V(\Psi) = \frac{1}{2}m_\Psi^2\Psi^2,$$

where m_Ψ is the mass of the scalar field.

3 Gravitational Decoupling

Equations (7)-(10) form a system of non-linear differential equations with eight unknowns: two metric potentials (v, χ), five matter variables ($\rho, p, \Theta_0^0, \Theta_1^1, \Theta_2^2$) and a massive scalar field. In order to evaluate the unknown functions, we implement the novel technique of EGD [17] on SBD field equations. This technique determines the effect of Θ_δ^γ on the matter distribution by inducing the following deformations in the metric potentials

$$v(r) \mapsto \mu(r) + \alpha g(r), \quad (11)$$

$$e^{-\chi(r)} \mapsto e^{-\eta(r)} + \alpha f(r), \quad (12)$$

where $f(r)$ and $g(r)$ encode the translations in radial and temporal metric components, respectively. Moreover, the free parameter α controls the contribution of deformations. It is noteworthy that spherical symmetry of the compact object is preserved under these geometric deformations. Substituting the deformed metric potentials in Eqs.(7)-(9) splits the system into two sets. The first set corresponds to $\alpha = 0$ and exclusively describes the isotropic configuration as

$$\begin{aligned} \rho &= \frac{1}{2r^2\Psi(r)} \left\{ e^{-\eta(r)} \left(r^2 e^{\eta(r)} V(\Psi)\Psi(r) + r^2(-\omega_{BD})\Psi'^2(r) + ((r\eta'(r) \right. \right. \\ &\quad \left. \left. - 4)\Psi'(r) - 2r\Psi''(r))r\Psi(r) + 2\Psi^2(r)(r\eta'(r) + e^{\eta(r)} - 1) \right) \right\}, \end{aligned} \quad (13)$$

$$\begin{aligned} p &= \frac{1}{2} \left\{ \frac{1}{r^2\Psi(r)} \left(e^{-\eta(r)} \left(-r^2\omega_{BD}\Psi'^2(r) + \Psi^2(r)(2r\mu'(r) - 2e^{\eta(r)} + 2) \right. \right. \right. \\ &\quad \left. \left. + r\Psi(r)(r\mu'(r) + 4)\Psi'(r) \right) - V(\Psi) \right\}, \end{aligned} \quad (14)$$

$$\begin{aligned} p &= \frac{1}{4r\Psi(r)} \left\{ e^{-\eta(r)} \left(2\Psi(r)(\Psi'(r)(r\mu'(r) - r\eta'(r) + 2) + 2r\Psi''(r)) + \Psi^2(r) \right. \right. \\ &\quad \left. \left. \times (2r\mu''(r) + \mu'(r)(2 - r\eta'(r)) + r\mu'^2(r) - 2\eta'(r)) - 2re^{\eta(r)}\Psi(r)V(\Psi) \right) \right\} \end{aligned}$$

$$+ 2r\omega_{BD}\Psi'^2(r))\}. \quad (15)$$

The conservation of isotropic matter distribution in (μ, η) coordinates is represented by the conservation equation

$$T_1^{1'(\text{eff})} - \frac{\mu'(r)}{2}(T_0^{0(\text{eff})} - T_1^{1(\text{eff})}) = 0. \quad (16)$$

The second set containing evolution equations for the anisotropic source is given as

$$\begin{aligned} \Theta_0^0 &= \frac{-1}{2r^2\Psi(r)} \{ (r\Psi(r)f'(r)(r\Psi'(r) + 2\Psi(r)) + f(r)(r^2\omega_{BD}\Psi'^2(r) \\ &+ 2r\Psi(r)(r\Psi''(r) + 2\Psi'(r)) + 2\Psi^2(r))) \}, \end{aligned} \quad (17)$$

$$\begin{aligned} \Theta_1^1 &= \frac{-f(r)}{2r^2\Psi(r)} (-r^2\omega_{BD}\Psi'^2(r) + r\Psi(r)(rv'(r) + 4)\Psi'(r) + 2\Psi^2(r)(rv'(r) \\ &+ 1)) - \frac{e^{-\eta(r)}g'(r)(r\Psi'(r) + 2\Psi(r))}{2r}, \end{aligned} \quad (18)$$

$$\begin{aligned} \Theta_2^2 &= \frac{-f(r)}{4r\Psi(r)} (2\Psi(r)((rv'(r) + 2)\Psi'(r) + 2r\Psi''(r)) + \Psi^2(r)(2rv''(r) \\ &+ rv'^2(r) + 2v'(r)) + 2r\omega_{BD}\Psi'^2(r)) - \frac{f'(r)}{4r} (\Psi(r)(rv'(r) + 2) \\ &+ 2r\Psi'(r)) - \frac{e^{-\eta(r)}}{4r} (2rg'(r)\Psi'(r) + \Psi(r)(2rg''(r) + \alpha rg'^2(r) + g'(r) \\ &\times (2r\mu'(r) - r\eta'(r) + 2))). \end{aligned} \quad (19)$$

The divergence of the source Θ_δ^γ leads to

$$\Theta_1^{1'(\text{eff})} - \frac{v'(r)}{2}(\Theta_0^{0(\text{eff})} - \Theta_1^{1(\text{eff})}) - \frac{2}{r}(\Theta_2^{2(\text{eff})} - \Theta_1^{1(\text{eff})}) = \frac{g'(r)}{2}(T_0^{0(\text{eff})} - T_1^{1(\text{eff})}), \quad (20)$$

where

$$\begin{aligned} \Theta_0^{0(\text{eff})} &= \frac{1}{\Psi} \left(\Theta_0^0 + \frac{1}{2}f'(r)\Psi'(r) + f(r)\Psi'' + \frac{\omega_{BD}f(r)\Psi'^2}{2\Psi} + \frac{2f(r)\Psi'(r)}{r} \right), \\ \Theta_1^{1(\text{eff})} &= \frac{1}{\Psi} \left(\Theta_1^1 + \frac{1}{2r\Psi}e^{-\eta(r)}\Psi'(r) (f(r)e^{\eta(r)} (\Psi(r)(rv'(r) + 4) - r\omega_{BD} \right. \\ &\times \Psi'(r)) + r\Psi(r)g'(r)), \end{aligned}$$

$$\begin{aligned}\Theta_2^{2(\text{eff})} &= \frac{1}{\Psi} \left(\Theta_2^2 + \frac{1}{2r\Psi} e^{-\eta(r)} (r\Psi(r)\Psi'(r) (e^{\eta(r)} f'(r) + g'(r)) + f(r) \right. \\ &\times \left. e^{\eta(r)} (\Psi(r) ((rv'(r) + 2) \Psi'(r) + 2r\Psi''(r)) + r\omega_{BD}\Psi'^2(r)) \right).\end{aligned}$$

The conservation equation of the energy-momentum tensor $T_\delta^{\gamma(\text{eff})}$ in (v, χ) -coordinate system yields

$$\nabla_\gamma T_\beta^{\gamma(\text{eff})} = \nabla_\gamma^{(\mu, \eta)} T_\beta^{\gamma(\text{eff})} - \frac{g'(r)}{2} (T_0^{0(\text{eff})} - T_1^{1(\text{eff})}) \delta_\beta^1, \quad (21)$$

where $\nabla_\gamma^{(\mu, \eta)}$ represents the divergence of a tensor in (μ, η) -frame. As a direct consequence of Eqs.(16) and (20), we have

$$\nabla_\gamma^{(\mu, \eta)} T_\beta^{\gamma(\text{eff})} = 0, \quad \nabla_\gamma \Theta_\beta^{\gamma(\text{eff})} = \frac{g'(r)}{2} (T_0^{0(\text{eff})} - T_1^{1(\text{eff})}) \delta_\beta^1. \quad (22)$$

Equations (21) and (22) imply that exchange of energy takes place between the sources $T_{\gamma\delta}^{(m)}$ and $\Theta_{\gamma\delta}$ but the overall energy and momentum of the system remain unchanged. Thus, these sources can be decoupled provided that energy can be transferred from one setup to the other. However, if $T_{\gamma\delta}^{(m)}$ represents either a vacuum solution or a barotropic fluid, matter sources interacting only gravitationally can also be decoupled via EGD approach. It is worthwhile to mention here that in the specific case of MGD ($g(r) = 0$), there is no exchange of matter between the isotropic and anisotropic configurations.

4 Anisotropic Solutions

When we apply the EGD technique, the system (7)-(9) is decomposed into two sets: Eqs.(13)-(15) represent the seed source in terms of $T_{\gamma\delta}^{(m)}$, μ and η whereas the influence of the additional source is determined by the second set (17)-(19) with five unknowns ($g(r)$, $f(r)$, Θ_0^0 , Θ_1^1 , Θ_2^2). The undetermined variables of the second set can be evaluated if a viable solution for the isotropic sector is known. Thus, EGD approach has simplified the process of extracting solutions of the field equations by reducing the degrees of freedom from 4 to 2. In this section, we obtain anisotropic analogues of two solutions: Tolman IV and KB.

In 1939, Tolman [42] constructed eight static spherically symmetric solutions for perfect fluid and explored the conditions for smooth matching of interior and exterior geometries. Tolman IV is one of the physically acceptable solutions [43] which corresponds to a non-vanishing surface density. It has previously been employed to investigate different features of self-gravitating systems [19, 44]. The line element of Tolman IV solution is written as

$$ds^2 = B^2 \left(1 + \frac{r^2}{A^2}\right) dt^2 - \frac{1 + \frac{2r^2}{A^2}}{\left(1 + \frac{r^2}{A^2}\right)\left(1 - \frac{r^2}{F^2}\right)} dr^2 - r^2(d\theta^2 + \sin^2\theta d\phi^2), \quad (23)$$

where the constants A , B and F are determined through the matching of internal and external spacetimes at the boundary (Σ) of the celestial object. The Schwarzschild metric describes vacuum in the exterior of the celestial object as

$$ds^2 = \left(1 - \frac{2M}{r}\right) dt^2 - \frac{1}{\left(1 - \frac{2M}{r}\right)} dr^2 - r^2(d\theta^2 + \sin^2\theta d\phi^2), \quad (24)$$

where M represents the overall mass of the compact structure. The junction conditions that ensure smooth matching of internal and external geometries at the stellar boundary ($r = R =$ radius of compact object) are expressed as

$$\begin{aligned} (g_{\gamma\delta}^-)_{\Sigma} &= (g_{\gamma\delta}^+)_{\Sigma}, & (p_r)_{\Sigma} &= 0, \\ (\Psi^-(r))_{\Sigma} &= (\Psi^+(r))_{\Sigma}, & (\Psi'^-(r))_{\Sigma} &= (\Psi'^+(r))_{\Sigma}. \end{aligned}$$

The junction conditions evaluate the constants A , B and F (for $\alpha = 0$) as

$$A^2 = -\frac{R^2 (R^2\zeta + M(28R - 2R\zeta) + 2M^2(\omega_{BD} - 12) - 8R^2)}{R\zeta(R - 2M) + 2M^2\omega_{BD}}, \quad (25)$$

$$B^2 = \frac{(R - 2M)(3R^2\zeta - 6M(R\zeta + 10R) + 6M^2(\omega_{BD} + 12) + 8R^2)}{2R(R^2\zeta - 2M(R\zeta + 11R) + 2M^2(\omega_{BD} + 12) + 4R^2)}, \quad (26)$$

$$\begin{aligned} F^2 &= (4R^3(3M - 2R)(\zeta + 4))(m_{\Psi}^4 R^6 + 4R^2\zeta + M^2(4m_{\Psi}^4 R^4 + 2\zeta(\omega_{BD} \\ &+ 12) + 8(\omega_{BD} + 12)) - 4M(m_{\Psi}^4 R^5 + 6R\zeta + 16R))^{-1}. \end{aligned} \quad (27)$$

where $\zeta = m_{\Psi}^2 R^2 \sqrt{1 - \frac{2M}{R}}$.

Krori and Barua [45] formulated a physically acceptable solution for a static charged sphere. The highlight of this solution is that no restrictions are imposed on the metric functions to avoid singularities, i.e., it is regular

throughout the spacetime. This solution has proved helpful in checking the impact of electromagnetic field on matter source. However, researchers have also employed this ansatz to inspect physical characteristics of uncharged systems [46]. The KB solution is defined by the following line element

$$ds^2 = e^{ar^2+b} dt^2 - e^{cr^2} dr^2 - r^2(d\theta^2 + \sin^2 \theta d\phi^2), \quad (28)$$

where the constants a , b and c are evaluated (for $\alpha = 0$) through the matching conditions as

$$a = \frac{R\zeta(R-2M) + 2M^2\omega_{BD}}{4R^2(R-2M)(2R-3M)}, \quad (29)$$

$$b = \frac{R\zeta(R-2M) + 2M^2\omega_{BD}}{-4(6M^2 - 7MR + 2R^2)} + \ln\left(1 - \frac{2M}{R}\right), \quad (30)$$

$$c = -\frac{\ln\left(1 - \frac{2M}{R}\right)}{R^2}. \quad (31)$$

The anisotropic model is completely specified by the following matter variables

$$\begin{aligned} \rho &= \frac{e^{-\eta(r)}}{2r^2\Psi(r)} \left(-r\Psi(r) \left(\Psi'(r) (\alpha r e^{\eta(r)} f'(r) + 4\alpha f(r)e^{\eta(r)} - r\eta'(r) + 4) \right. \right. \\ &+ 2r\Psi''(r) (\alpha f(r)e^{\eta(r)} + 1)) - 2\Psi^2(r) (\alpha r e^{\eta(r)} f'(r) + \alpha f(r)e^{\eta(r)} \\ &- r\eta'(r) - e^{\eta(r)} + 1) + r^2(-\omega_{BD})\Psi'^2(r) (\alpha f(r)e^{\eta(r)} + 1) \\ &+ r^2 e^{\eta(r)} \Psi(r) V(\Psi) \Big), \end{aligned} \quad (32)$$

$$\begin{aligned} p_r &= \frac{\Psi(r)}{r^2} \left((\alpha f(r) + e^{-\eta(r)}) (\alpha r g'(r) + r\mu'(r) + 1) - 1 \right) - \frac{1}{2r\Psi(r)} \\ &\times \left(\Psi'(r) (\alpha f(r) + e^{-\eta(r)}) (r\omega_{BD}\Psi'(r) - \Psi(r) (\alpha r g'(r) + r\mu'(r) + 4)) \right) \\ &- \frac{V(\Psi)}{2}, \end{aligned} \quad (33)$$

$$\begin{aligned} p_\perp &= (\alpha f(r) + e^{-\eta(r)}) \left(\frac{1}{2}\Psi'(r) \left(\frac{\alpha e^{\eta(r)} f'(r) - \eta'(r)}{\alpha f(r)e^{\eta(r)} + 1} + \alpha g'(r) + \mu'(r) \right. \right. \\ &+ \left. \left. \frac{2}{r} \right) + \Psi''(r) + \frac{\omega_{BD}\Psi'^2(r)}{2\Psi(r)} \right) + \frac{1}{2}\Psi(r) (\alpha f(r) + e^{-\eta(r)}) \left((\alpha e^{\eta(r)} f'(r) \right. \\ &- \left. \eta'(r)) (\alpha g'(r) + \mu'(r)) \right) (2\alpha f(r)e^{\eta(r)} + 2)^{-1} + \frac{1}{r} \left(\frac{\alpha e^{\eta(r)} f'(r) - \eta'(r)}{\alpha f(r)e^{\eta(r)} + 1} \right) \end{aligned}$$

$$+ \alpha g'(r) + \mu'(r)) + \alpha g'' + \frac{1}{2} (\alpha g'(r) + \mu'^2(r)) + \mu''(r) \Big) - \frac{V(\Psi)}{2}, \quad (34)$$

with anisotropy $\Delta = p_\perp - p_r$.

In order to extend the seed solutions to the anisotropic domain, we require two constraints on Θ_δ^γ to close the anisotropic system. For this purpose, we choose a mimic constraint

$$\Theta_1^1(r) = p(r), \quad (35)$$

which fulfills the requirement of vanishing pressure at the hypersurface. Under this constraint, the values of the constants F and a remain unchanged. The remaining constants A and c appear as free parameters in corresponding extended versions whose values are chosen as presented in Eqs.(25) and (29), respectively. For the second constraint, a linear EoS as well as a regularity condition on anisotropy is implemented which will be discussed in subsections 4.1 and 4.2, respectively.

The limits enforced by the weak-field on values of the coupling parameter can be avoided through a lower bound for mass of the scalar field ($m_\Psi > 10^{-4}$ in dimensionless units). In accordance with this limit, we take $m_\Psi = 0.01$ and solve the wave equation numerically to determine the massive scalar field. Different features of anisotropic models are investigated graphically for three values of α (0.2, 0.55, 0.9) by employing the observed mass ($1.97M_\odot$) and radius (11.29km) of the star PSR J1614-2230.

4.1 Case I: Linear Equation of State

We consider a linear EoS for the source Θ_δ^γ as

$$\Theta_0^0 = \chi \Theta_1^1 + \psi \Theta_2^2. \quad (36)$$

Setting $\chi = 1$ and $\psi = 0$ in the above equation leads to

$$\begin{aligned} & \frac{e^{-\eta(r)}}{r\Psi(r)} \left(-r\Psi(r) (\Psi'(r) (re^{\eta(r)} f'(r) + 4f(r)e^{\eta(r)} + r\mu'(r) + 4) + 2rf(r) \right. \\ & \times e^{\eta(r)} \Psi''(r)) - 2\Psi^2(r) (re^{\eta(r)} f'(r) + f(r)e^{\eta(r)} + r\mu'(r) - e^{\eta(r)} + 1) \\ & \left. + r^2(-\omega_{BD}) (f(r)e^{\eta(r)} - 1) \Psi'^2(r) + r^2 e^{\eta(r)} \Psi(r) V(\Psi) \right) = 0, \end{aligned} \quad (37)$$

which is solved numerically for $f(r)$ along with the wave equation with the central conditions $\Psi(0) = 0.2$, $\Psi'(0) = 0$ and $f(0) = 0$. On the other hand,

the mimic constraint (35) yields the following temporal geometric function

$$\begin{aligned}
g(r) = & \int \left((r^2 \omega_{BD} (f(r)e^{\eta(r)} + 1) \Psi'(r)^2 - r\Psi(r) (f(r)e^{\eta(r)} + 1) (r\mu'(r) \right. \\
& + 4) \Psi'(r) - 2\Psi^2(r) (f(r)e^{\eta(r)} (r\mu'(r) + 1) + r\mu'(r) - e^{\eta(r)} + 1) \\
& \left. + r^2 e^{\eta(r)} \Psi(r) V(\Psi)) (r\Psi(r) (r\Psi'(r) + 2\Psi(r)) (\alpha f(r)e^{\eta(r)} + 1))^{-1} \right) dr.
\end{aligned} \tag{38}$$

Substituting the metric functions and constants corresponding to Tolman IV solution in Eqs.(32)-(34), (37) and (38) provides the extended version of this solution.

The graphical analysis of state determinants is provided in Figure 1 with $\omega_{BD} = 9.87$. A stellar model is well-behaved if the state parameters are positive, finite and decrease monotonically away from the center. Moreover, radial pressure must vanish at the boundary of the star. It is observed from Figure 1 that energy density as well as pressure components are positive throughout and maximum at the center for $\alpha = 0.2$ and 0.55 . However, for $\alpha = 0.9$, the transverse pressure increases monotonically instead of decreasing. The anisotropy is zero at the center and increases towards the surface indicating the presence of an outward repulsive force. It is noted that higher values of α increase the density and repulsive force in the interior of the structure whereas the pressure components decrease.

Four energy bounds on matter variables distinguish normal matter from exotic material. Since stellar structures are composed of ordinary matter, it is crucial that the parameters governing the interior of compact objects obey these energy conditions. The null, weak, strong and dominant energy conditions in the framework of SBD theory are, respectively, expressed as [47]

$$\begin{aligned}
\text{NEC: } & \rho + p_r \geq 0, \quad \rho + p_\perp \geq 0, \\
\text{WEC: } & \rho \geq 0, \quad \rho + p_r \geq 0, \quad \rho + p_\perp \geq 0, \\
\text{SEC: } & \rho + p_r + 2p_\perp \geq 0, \\
\text{DEC: } & \rho - p_r \geq 0, \quad \rho - p_\perp \geq 0.
\end{aligned}$$

The first three conditions are readily satisfied for extended Tolman IV solution as energy density and pressure (radial/transverse) are positive within the compact object. Figure 2 demonstrates that the parameters governing the matter source agree with DEC ensuring viability of the model.

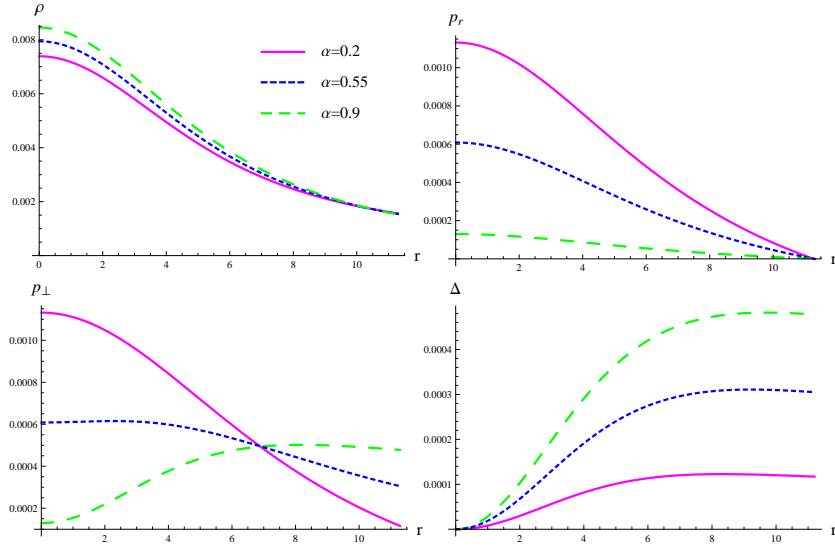


Figure 1: Plots of matter variables and anisotropy of extended Tolman IV solution for case I.

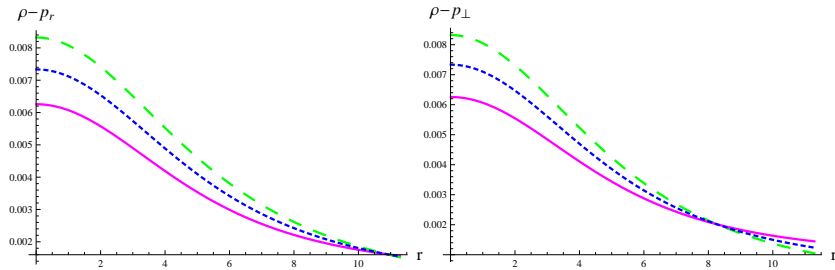


Figure 2: DEC for anisotropic Tolman IV with case I.

Another important physical feature of a self-gravitating system is its compactness ($u(r)$) in a state of equilibrium. The compactness factor is defined as the relation of mass to the radius of the object. Buchdahl [48] calculated the upper limit of this parameter for a fluid with non-increasing energy density by matching the interior of a static sphere to Schwarzschild exterior solution. This limit is given as

$$u(r) = \frac{m}{R} < \frac{4}{9},$$

where $m(r) = \frac{R}{2}(1 - e^{-\chi})$. The compactness factor obtained for anisotropic Tolman IV solution (shown in Figure 3) conforms to Buchdahl limit. The surface redshift ($Z(r)$) of a celestial object gauges the increase in wavelength of electromagnetic radiation due to gravitational force exerted by the star. It is defined as

$$Z(r) = \frac{1}{\sqrt{1 - 2u}} - 1.$$

For a perfect fluid distribution, Buchdahl limit restricts the value of redshift at the stellar surface as $Z(r) < 2$. However, for an anisotropic configuration, the upper limit of surface redshift changes to 5.211 [49]. It is observed from Figure 3 that the range of redshift parameter complies with the above limit.

The internal structure of compact objects is determined by the gravitational (M_g) as well as baryonic (M_b) mass. The gravitational mass of a spherical gravitationally bound system is measured using Kepler's law (when a satellite orbits the star) and is defined as

$$M_g = \frac{1}{2} \int_0^R \rho r^2 dr. \quad (39)$$

The gravitational mass associated with the anisotropic star is obtained by numerically solving the above equation along with the Eqs.(10) and (37) under the condition $M_g(0) = 0$. The mass is presented in Figure 4 as a function of radius for chosen values of α . It is noted that the gravitational mass of the spherical system increases with an increase in the decoupling parameter. On the other hand, baryonic mass is directly related to the massive iron core at the center of the stellar remnant and is defined as the volume integral of baryon number density times mass of a baryon. Burrows

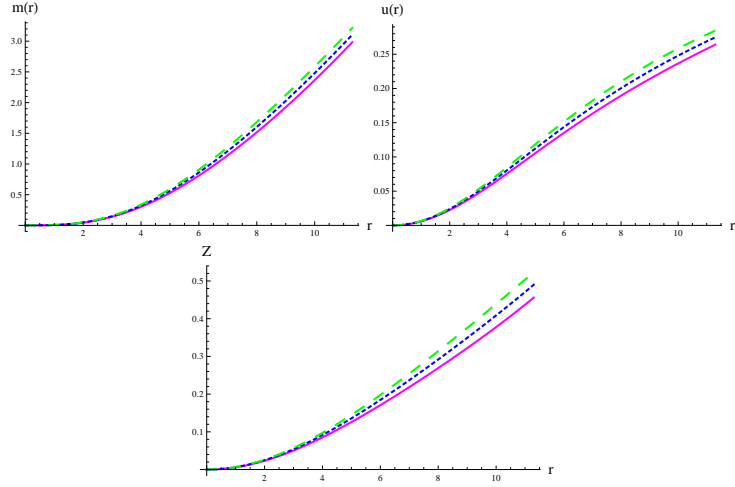


Figure 3: Plots of mass, compactness and redshift parameters corresponding to anisotropic Tolman IV for case I.

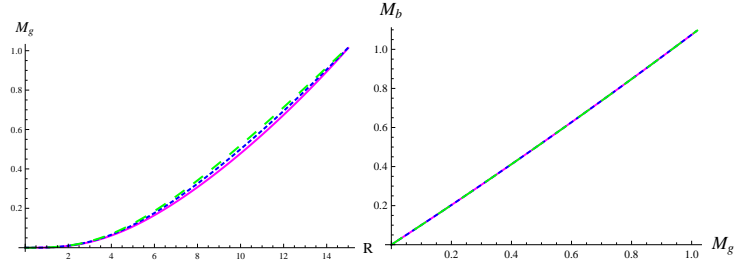


Figure 4: Plots of gravitational mass versus radius (left) and baryonic mass versus gravitational mass (right) corresponding to anisotropic Tolman IV with case I.

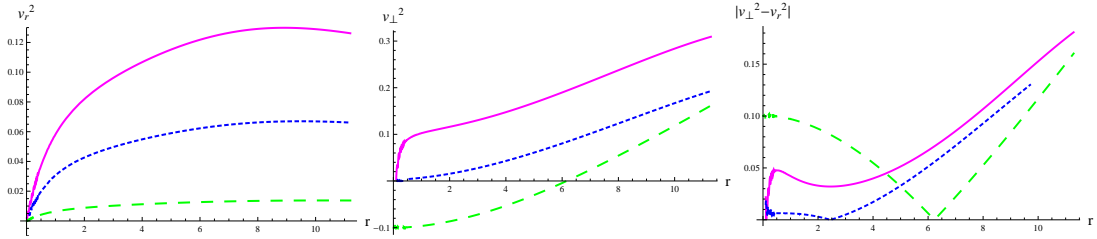


Figure 5: Plots of radial/tangential velocities and $|v_{\perp}^2 - v_r^2|$ corresponding to anisotropic Tolman IV for case I.

and Lattimer [50] provided the relation between gravitational and baryonic mass as

$$M_b = M_g + \varpi M_g^2, \quad (40)$$

where $\varpi = 0.075$ for a large number of nuclear EoS [51]. The relation between gravitational and baryonic masses, presented in Figure 4, shows that maximum baryonic mass is attained for $\alpha = 0.9$.

The stability of the constructed model is investigated through causality condition which states that the speed of a propagating wave is always less than the speed of light [52]. Thus, according to this criterion the radial ($v_r^2 = \frac{dp_r}{dp}$) and tangential ($v_\perp^2 = \frac{dp_\perp}{dp}$) components of sound speed must lie within the interval $(0, 1)$. The plots in Figure 5 clearly show that the anisotropic model is stable for $\alpha = 0.2, 0.55$ whereas tangential velocity becomes positive after a certain distance corresponding to $\alpha = 0.9$. Herrera's cracking approach [53] is another method for determining the stability of the stellar model. A system is stable with respect to this concept if the inward directed radial forces of a perturbed system maintain the same direction throughout the setup, i.e., a region is stable if radial/tangential components of velocity satisfy the relation $0 < |v_\perp^2 - v_r^2| < 1$. The extended Tolman IV solution complies with this condition for $\alpha = 0.2, 0.55$ as shown in Figure 5.

The anisotropic version of the KB solution is formulated in SBD gravity through Eqs.(28), (32)-(34), (37) and (38). Plots of state variables are presented in Figure 6 for $\omega_{BD} = 9.87$. The profiles of energy density and pressure components attain maximum value at the center and decrease towards the surface for $\alpha = 0.2$. However, for higher values of the decoupling parameter (0.55, 0.9), tangential pressure exhibits monotonically increasing behavior. Furthermore, the anisotropy vanishes at the center as required. This anisotropic solution is consistent with all energy bounds for chosen values of α (Figure 7) leading to a viable configuration. The compactness factor and surface redshift obey the desired restraints as shown in Figure 8. Figure 9 shows an increment in the gravitational mass as α increases from 0.2 to 0.55. However, a drop in the mass is observed for a higher value of α . Moreover, the baryonic mass is maximum for $\alpha = 0.55$. The anisotropic model violates the causality condition as tangential velocity is negative throughout the system for selected values of α (refer to Figure 10). However, the compact object is stable with respect to Herrera's cracking approach.

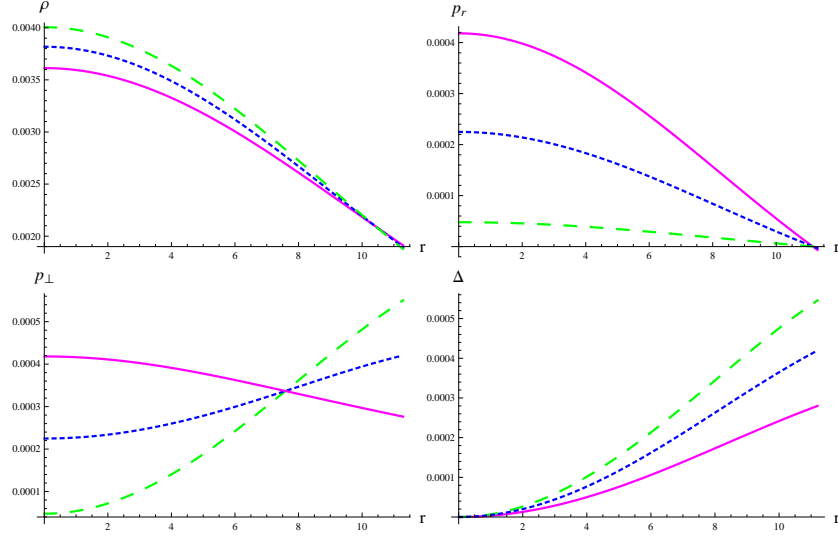


Figure 6: Plots of matter variables and anisotropy of extended KB solution for case I.

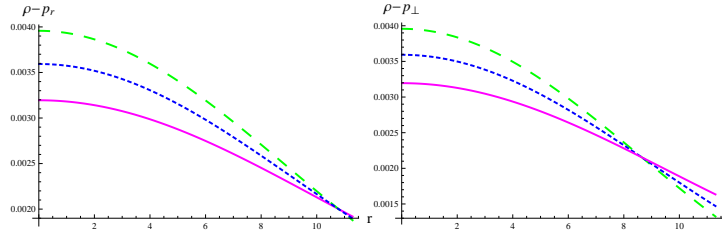


Figure 7: DEC for extended KB solution with case I.

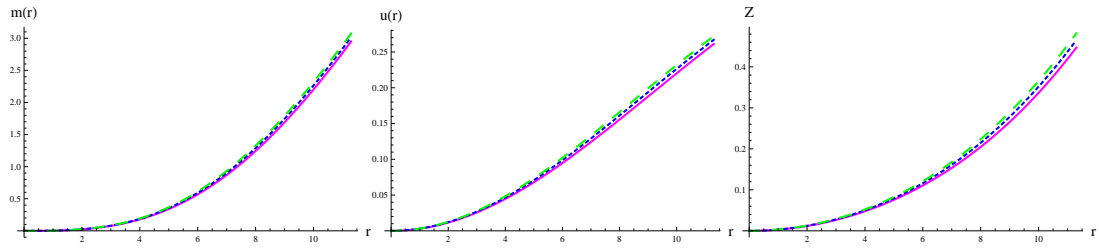


Figure 8: Plots of mass, compactness and redshift parameters corresponding to extended KB solution for case I.

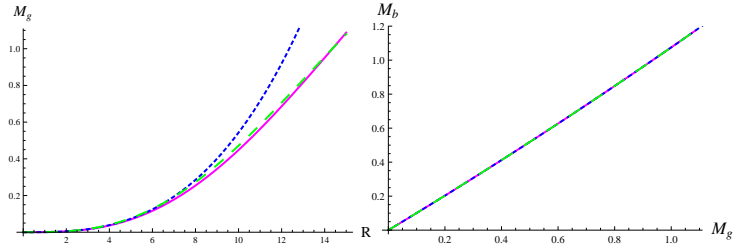


Figure 9: Plots of gravitational mass versus radius (left) and baryonic mass versus gravitational mass (right) for extended KB solution with case I.

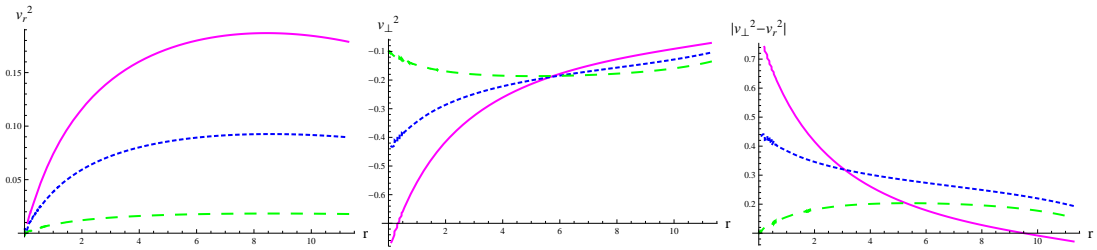


Figure 10: Plots of radial/tangential velocities and $|v_\perp^2 - v_r^2|$ for extended KB solution with case I.

4.2 Case II: Regularity Condition on Anisotropy

Bowers and Liang [54] proposed that singularities in the Tolman-Oppenheimer-Volkoff equation can be avoided if the following condition is imposed on the anisotropy

$$p_{\perp} - p_r = Ch(p_r, r)(\rho + p_r)r^n,$$

where the parameter C measures the strength of the anisotropy and $n > 1$. For the present work, we have taken $C = -0.5$. Moreover, h is an arbitrary function of radial pressure and contains information about the anisotropy of the system. In 1981, Cosenza et al. [55] evaluated anisotropic solutions from known isotropic solutions by assuming the energy density of a perfect fluid and taking $h(p_r, r) = \frac{v'(r)}{2}r^{1-n}$. These conditions have already been employed in MGD approach to obtain new anisotropic solutions [56, 57]. In this section, we obtain anisotropic analogues of seed solutions by imposing Bowers-Liang constraint on Θ -sector as

$$\Theta_2^2 - \Theta_1^1 = Ch(\Theta_1^1, r)(-\Theta_0^0 + \Theta_1^1)r^n, \quad (41)$$

with $h(\Theta_1^1, r) = \frac{v'(r)}{2}r^{1-n}$. Substituting Eqs.(17)-(19) in the above equation leads to

$$\begin{aligned} & \frac{e^{-\eta(r)}}{r\Psi(r)} \left(f(r)e^{\eta(r)} (r\Psi(r) (\Psi'(r) (C\alpha r^2 g'(r)v'(r) + Cr^2 \mu'(r)v'(r) + 4) \right. \\ & - 2r\Psi''(r) (Cr v'(r) + 2)) + \Psi^2(r) (-2(\alpha r^2 g''(r) + r^2 \mu''(r) - 2) \\ & + \alpha^2 r^2 g'^2(r) + 2\alpha r g'(r) (r\mu'(r) - Cr v'(r) - 1) + r^2 \mu'^2(r) - 2r\mu'(r) \\ & \times (Cr v'(r) + 1))) - 2r^2 \omega_{BD} \Psi'^2(r) (Cr v'(r) + 2) - r\Psi(r) (r\Psi'(r) \\ & \times (e^{\eta(r)} f'(r) (Cr v'(r) + 2) - Cr g'(r)v'(r)) + \Psi(r) (e^{\eta(r)} f'(r) (\alpha r g'(r) \\ & + r\mu'(r) + 2Cr v'(r) + 2) + 2r g''(r) + \alpha r g'^2(r) + g'(r) (2r\mu'(r) - r\eta'(r) \\ & \left. - 2Cr v'(r) - 2))) \right) = 0. \end{aligned} \quad (42)$$

We obtain the deformation function $g(r)$ by simultaneously solving Eqs.(3) and (42) numerically with the initial conditions $\Psi(0) = 0.1$, $\Psi'(0) = 0$, $g(0) = 0$ and $g'(0) = 0.5$. The function $f(r)$ is evaluated from the constraint (35) as

$$\begin{aligned} f(r) &= e^{-\eta(r)} (2\Psi^2(r) (-r g'(r) - r\mu'(r) + e^{\eta(r)} - 1) - r\Psi(r)\Psi'(r) (r g'(r) \\ & + r\mu'(r) + 4) + r^2 e^{\eta(r)} \Psi(r) V(\Psi) + r^2 \omega_{BD} \Psi'^2(r)) (r\Psi(r)\Psi'(\alpha r g'(r) \\ & + r\mu'(r) + 4) + 2\Psi^2(r) (\alpha r g'(r) + r\mu'(r) + 1) - r^2 \omega_{BD} \Psi'^2(r))^{-1}. \end{aligned} \quad (43)$$

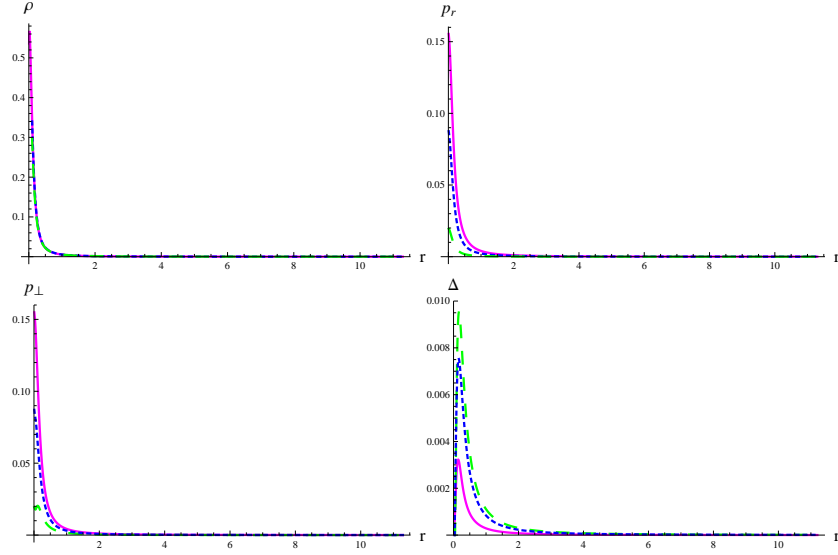


Figure 11: Plots of matter variables and anisotropy of extended Tolman IV for case II.

Tolman IV solution is extended via constraint (41) by employing the associated constants in Eqs.(32)-(34), (42) and (43). The physical characteristics of this solution are investigated graphically for $\omega_{BD} = 17.95$. Figure 11 displays the energy density and pressures as decreasing functions of r for the considered values of α . A decrease in the physical parameters (ρ , p_r , p_{\perp}) is observed for higher values of the decoupling parameter whereas anisotropy increases as α increases. Moreover, the anisotropy within the star increases for some distance and then decreases indicating the presence of a weaker repulsive force near the stellar surface. Figure 12 shows that the system corresponding to extended Tolman IV solution is viable as it adheres to the restrictions imposed by energy bounds. Moreover, the compactness and redshift parameters (Figure 13) adhere to the respective bounds. The gravitational and baryonic masses calculated from Eqs.(39) and (40), respectively are plotted in Figure 14. The compact structure becomes more massive as α increases from 0.2 to 0.55 but decreases for $\alpha = 0.9$. Furthermore, the model has maximum baryonic mass for $\alpha = 0.55$. Finally, the extended Tolman IV solution is stable for the considered values of the decoupling parameter as it complies with the causality condition and cracking approach as shown in Figure 15.

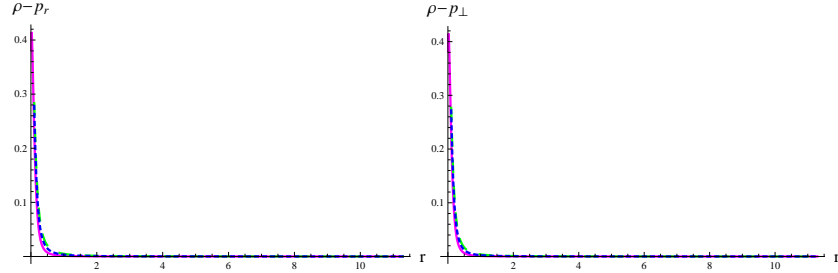


Figure 12: DEC for anisotropic Tolman IV with case II.

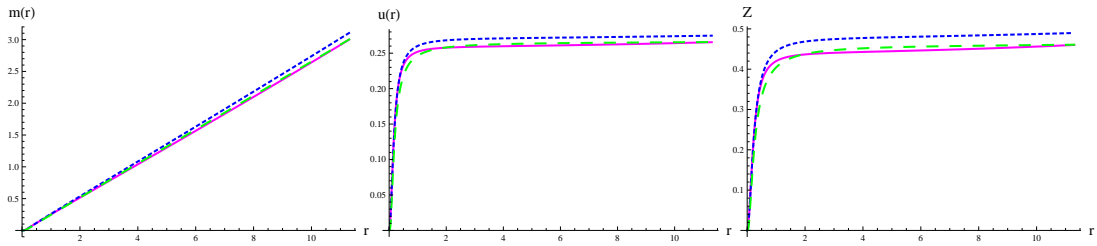


Figure 13: Plots of mass, compactness and redshift parameters corresponding to anisotropic Tolman IV for case II.

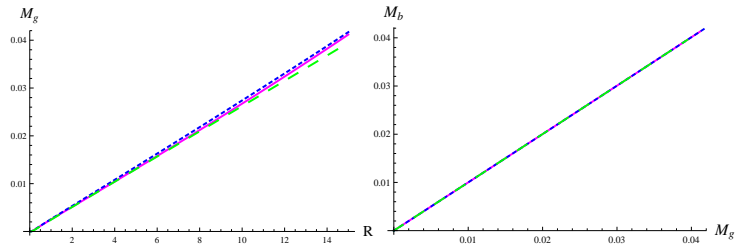


Figure 14: Plots of gravitational mass versus radius (left) and baryonic mass versus gravitational mass (right) corresponding to anisotropic Tolman IV for case II.

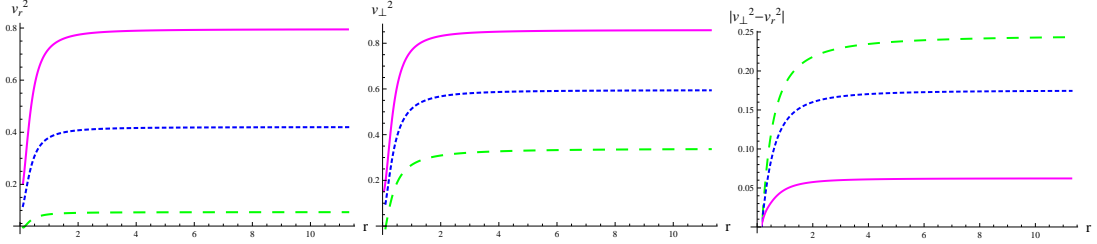


Figure 15: Plots of radial/tangential velocities and $|v_{\perp}^2 - v_r^2|$ corresponding to anisotropic Tolman IV for case II.

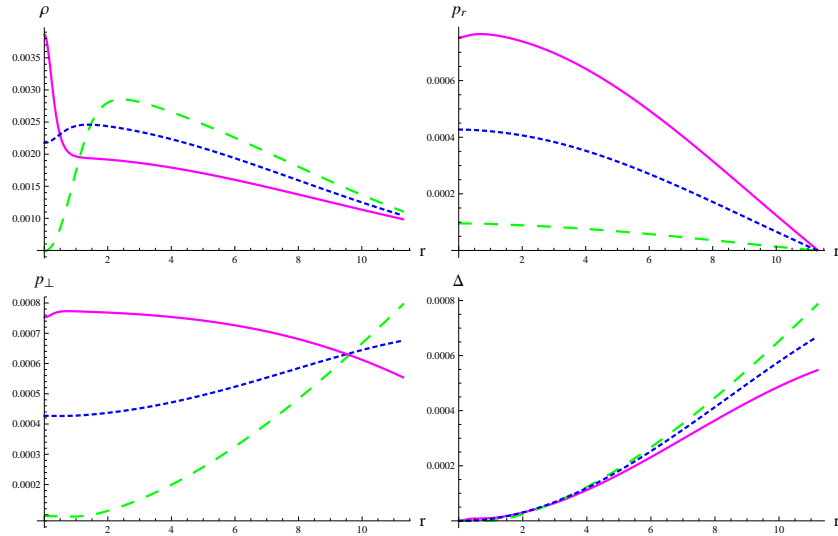


Figure 16: Plots of matter variables and anisotropy of extended KB solution for case II.

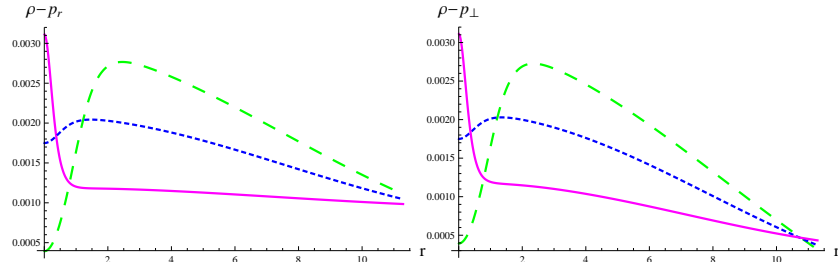


Figure 17: DEC for extended KB solution with case II.

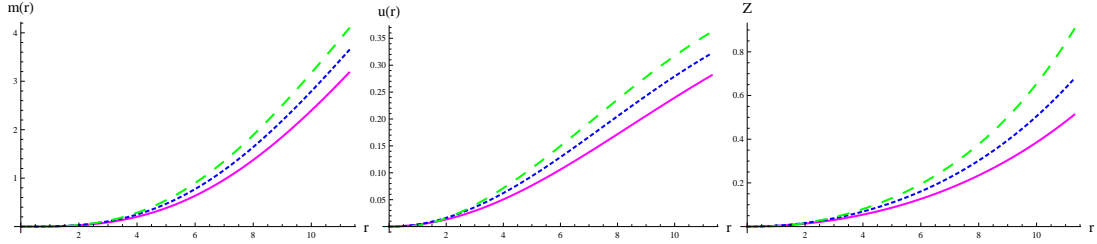


Figure 18: Plots of mass, compactness and redshift parameters corresponding to extended KB solution for case II.

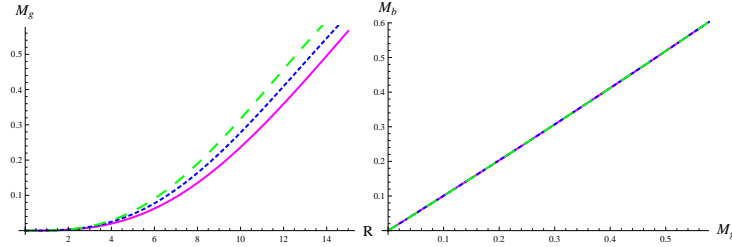


Figure 19: Plots of gravitational mass versus radius (left) and baryonic mass versus gravitational mass (right) corresponding to extended KB solution for case II.

The extended version of KB solution under Bowers-Liang constraint is constructed by plugging the associated metric potentials and constants in Eqs.(32)-(34), (42) and (43). It is noted from Figure 16 that energy density and tangential pressure are positive for the selected values of α but decrease monotonically only for $\alpha = 0.2$. However, the radial pressure has a maximum value at the center and vanishes at $r = R$ for all values of the decoupling parameter. Moreover, the state parameters are inversely proportional to α while the anisotropy is directly proportional to the decoupling parameter. The plots of DEC in Figure 17 show that the anisotropic solution is physically valid for the chosen values of α . The values of compactness parameter and surface redshift also lie in the desired range as displayed in Figure 18. The gravitational mass increases with increase in the decoupling parameter as shown in Figure 19. Moreover, the baryonic mass is maximum for $\alpha = 0.9$. The constructed model is stable only for $\alpha = 0.2$ as it violates causality and cracking conditions for higher values of the decoupling parameter (Figure 20).

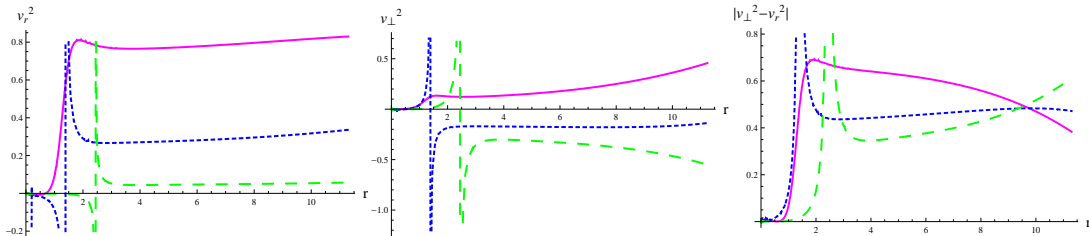


Figure 20: Plots of radial/tangential velocities and $|v_{\perp}^2 - v_r^2|$ corresponding to extended KB solution for case II.

5 Conclusions

In this paper, we have formulated anisotropic solutions by introducing a new source in the perfect fluid distribution in the framework of SBD gravity. For this purpose, the field equations have been decoupled into two sets via the EGD technique. To examine the efficiency of this method, we have specified the first set by considering metric coefficients of two isotropic solutions: Tolman IV and KB. The scalar field has been obtained by solving the wave equation numerically for $m_{\Psi} = 0.01$. The number of unknown variables in the anisotropic sector has been reduced through two constraints on the additional source. Finally, we have inspected physical properties of the constructed models through energy conditions, compactness and redshift parameters for $\alpha = 0.2, 0.55, 0.9$. The obtained solutions have also been checked for stability by employing two criteria: causality condition and Herrera's cracking approach.

The first condition on Θ -sector requires Θ_1^1 to mimic isotropic pressure. For the second constraint, we have discussed two cases:

- A barotropic EoS relating Θ_0^0 to Θ_1^1 ;
- A regularity condition on anisotropy on Θ_0^0 following Bowers-Lang constraint [54].

In the first scenario, the deformation functions $f(r)$ and $g(r)$ have been calculated through EoS and mimic constraint, respectively. The graphical analysis of state parameters of anisotropic Tolman IV solution shows that energy density and pressure components follow the accepted trend for $\alpha = 0.2, 0.55$ whereas transverse pressure monotonically increases for $\alpha = 0.9$. However,

the tangential pressure corresponding to the anisotropic KB solution decreases towards the boundary only for $\alpha = 0.2$. The anisotropic models represented by both solutions are viable as well as obey Buchdahl limit for compactness and redshift. Moreover, higher values of the decoupling parameter correspond to denser and more compact stellar structures in both models. The extended Tolman IV solution is stable for $\alpha = 0.2, 0.55$ whereas anisotropic KB solution is stable according to Herrera's cracking approach but violates the causality condition $0 \leq v_{\perp}^2 \leq 1$ for the considered values of α .

For case II, matter variables of the anisotropic version of Tolman IV solution are positive and decrease monotonically for the chosen values of α . On the other hand, the energy density of extended KB solution decreases monotonically only for $\alpha = 0.2$ while for $\alpha = 0.55, 0.9$, the density decreases after increasing for some distance. For these values of the decoupling parameter, tangential pressure increases towards the boundary. However, both solutions satisfy energy conditions as well as the limits on compactness and surface redshift. Moreover, increase in the decoupling parameter leads to a decrease in the density and compactness of both anisotropic models. Finally, the strength of the repulsive force due to positive anisotropy increases with the increase in α in all four solutions. The model corresponding to extended Tolman IV solution is consistent with both stability criteria whereas anisotropic KB solution is stable for $\alpha = 0.2$ only. It is inferred that viability of the extended Tolman IV solutions in GR [19, 56] is preserved in SBD gravity as well. Moreover, the anisotropic analogues of KB solution obtained here are viable for higher values of the decoupling parameter in contrast to the extended KB solutions obtained through MGD technique in [36]. Thus, EGD method yields anisotropic solutions with suitable physical properties. It is interesting to mention here that all the results of GR can be retrieved for $\Psi = \text{constant}$ and $\omega_{BD} \rightarrow \infty$.

Acknowledgment

This work has been supported by the *Pakistan Academy of Sciences Project*.

References

- [1] Schwarzschild, K.: Math. Phys. **189**(1916).

- [2] Lemaitre, G.: Ann. Soc. Sci. Bruxells A **53**(1993)51.
- [3] Ruderman, A.: Annu. Rev. Astron. Astrophys. **10**(1972)427.
- [4] Herrera, L. and Santos, N.O.: Phys. Reports **286**(1997)53.
- [5] Harko, T. and Mak, M.K.: Annalen Phys. **11**(2002)3.
- [6] Paul, B.C. and Deb, R.: Astrophys. Space Sci. **354**(2014)421.
- [7] Murad, M.H.: Astrophys. Space Sci. **20**(2016)361.
- [8] Ovalle, J.: Mod. Phys. Lett. A **23**(2008)3247.
- [9] Ovalle, J. and Linares, F.: Phys. Rev. D **88**(2013)104026.
- [10] Ovalle, J. et al.: Eur. Phys. J. C **78**(2018)122.
- [11] Gabbanelli, L., Rincon, A. and Rubio, C.: Eur. Phys. J. C **78**(2018)370.
- [12] Estrada, M. and Tello-Ortiz, F.: Eur. Phys. J. C **133**(2018)453.
- [13] Sharif, M. and Sadiq, S.: Eur. Phys. J. C **78**(2018)410.
- [14] Hensh, S. and Stuchlik, Z.: Eur. Phys. J. C **79**(2019)834.
- [15] Sharif, M. and Ama-Tul-Mughani, Q.: Int. J. Geom. Methods Mod. Phys. **16**(2019)1950187; Mod. Phys. Lett. A **35**(2020)2050091.
- [16] Casadio, R., Ovalle, J. and da Rocha, R.: Class. Quantum Grav. **32**(2015)215020.
- [17] Ovalle, J.: Phys. Lett. B **788**(2019)213.
- [18] Contreras, E. and Bargueño, P.: Class. Quantum Grav. **36**(2019)215009.
- [19] Sharif, M. and Ama-Tul-Mughani, Q.: Ann. Phys. **415**(2020)168122.
- [20] Sharif, M. and Ama-Tul-Mughani, Q.: Chinese J. Phys. **65**(2020)207.
- [21] Sharif, M. and Saba, S.: Eur. Phys. J. C **78**(2018)921; Sharif, M. and Waseem, A.: Ann. Phys. **405**(2019)14; Chin. J. Phys. **60**(2019)426; Sharif, M. and Saba, S., *Extended Gravitational Decoupling Approach in $f(\mathcal{G})$ Gravity*, Int. J. Mod. Phys. D (to appear, 2020), <https://doi.org/10.1142/S0218271820500418>.

- [22] Dirac, P.A.M: Nature **139**(1937)323; Proc. R. Soc. Lond. A **165**(1938)199.
- [23] Brans, C. and Dicke, R.H.: Phys. Rev. **124**(1961)3.
- [24] Weinberg, E.J.: Phys. Rev. D **40**(1989)3950.
- [25] Will, C.M.: Living Rev. Rel. **4**(2001)4.
- [26] Khoury, J. and Weltman, A.: Phys. Rev. D **69**(2004)044026.
- [27] Perivolaropoulos, L.: Phys. Rev. D **81**(2010)047501.
- [28] Buchdahl, H.A.: Int. J. Theor. Phys. **6**(1972)407.
- [29] Sneddon, G.E. and McIntosh, C.B.G.: Aust. J. Phys. **27**(1974)411.
- [30] Geroch, R.: J. Math. Phys. **12**(1971)918.
- [31] Bruckman, W.F. and Kazes, E.: Phys. Rev. D **16**(1977)2.
- [32] Goswami, G.K.: J. Math. Phys. **19**(1978)442.
- [33] Johri, V.B. and Goswami, G.K.: J. Math. Phys. **19**(1978)987; *ibid.* **21**(1980)2269.
- [34] Krori, K.D. and Bhattacharjee, D.R.: J. Math. Phys. **23**(1982)1846.
- [35] Riazi, N. and Askari, H.R.: Mon. Not. R. Astron. Soc. **261**(1993)229.
- [36] Sharif, M. and Majid, A.: Astrophys. Space Sci. **365**(2020)42.
- [37] Yazadjiev, S.S., Doneva, D.D. and Popchev, D.: Phys. Rev. D **93**(2016)084038.
- [38] Ramazanoğlu, F.M. and Pretorius, F.: Phys. Rev. D **93**(2016)064005.
- [39] Doneva, D.D. and Yazadjiev, S.S.: J. Cosmol. Astropart. Phys. **11**(2016)019.
- [40] Staykov, K.V. et al.: Eur. Phys. J. C **78**(2018)586.
- [41] Popchev, D. et al.: Eur. Phys. J. C **79**(2019)178.

- [42] Tolman, R.C.: Phys. Rev. **55**(1939)364.
- [43] Delgaty, M.S.R. and Lake, K.: Comput. Phys. Commun. **115**(1998)395.
- [44] Bhar, P., Singh, K.N. and Manna, T.: Astrophys. Space Sci. **361**(2016)284; Banerjee, S.: Pramana-J. Phys. **91**(2018)27.
- [45] Krori, K.D. and Barua, J.: J. Phys. A: Math. Gen. **8**(1975)4.
- [46] Momeni, D. et al.: Int. J. Mod. Phys. A **30**(2015)1550093; Zubair, M. and Abbas, G.: Astrophys. Space Sci. **361**(2016)342.
- [47] Fujii, Y. and Maeda, K.: *The Scalar-Tensor Theory of Gravitation* (Cambridge University Press, 2003).
- [48] Buchdahl, H.A.: Phys. Rev. D **116**(1959)1027.
- [49] Ivanov, B.V.: Phys. Rev. D **65**(2002)104011.
- [50] Burrows, A. and Lattimer, J.M.: Astrophys. J. **307**(1986)178; Lattimer, J.M. and Yahil, A.: Astrophys. J. **340**(1989)426.
- [51] Timmes, F.X., Woosley, S.E. and Weaver, T.A.: Astrophys. J. **457**(1996)834.
- [52] Abreu, H., Hernandez, H. and Nunez, L.A.: Class. Quantum Gravit. **24**(2007)4631.
- [53] Herrera, L.: Phys. Lett. A **165**(1992)206.
- [54] Bowers, R. and Liang, E.: Astrophys. J. **188**(1974)657.
- [55] Cosenza, M. et al.: J. of Math. Phys. **22**(1981)118.
- [56] Abellán, G.: Eur. Phys. J. C **80**(2020)177
- [57] Contreras, E., Tello-Ortiz, F. and Maurya, S.K.: arXiv:2002.12444.